

**IMPROVED TOPOLOGY FOR LINE-
COMMUTATED CONVERTER HVDC WITH
FOUR-POLE SYSTEM**

SABAH RAMADHAN MOHAMMED

UNIVERSITI SAINS MALAYSIA

2019

**IMPROVED TOPOLOGY FOR LINE-
COMMUTATED CONVERTER HVDC WITH
FOUR-POLE SYSTEM**

by

SABAH RAMADHAN MOHAMMED

**Thesis submitted in fulfilment of the
requirements for the degree of
Doctor of Philosophy**

July 2019

ACKNOWLEDGEMENT

I would like to thank my supervisor Assoc. Prof. Ir. Dr. Mohamad Kamarol who had given valuable guidance, support, advice, and encouragement throughout the course of my Ph. D. study. I want to express my gratitude to my supervisor, for offering me the opportunity to explore the challenging, for his support during this research work. I am also grateful to my co-supervisor Dr. Teh Jiashen who always been supportive. My thanks to all my teachers and lecturers throughout my study path from primary school to Ph.D.

Many thanks go to all staff members in the School of Electrical and Electronic Engineering, Universiti Sains Malaysia for their assistance, especially Power Lab technical staffs for their help and allowing me to access the facilities in the Power lab.

I would like to acknowledge the Universiti Sains Malaysia for funding me through the Bridging Grant under Grant 304.PELECT.6316098.

Finally, I am grateful to all my family members, my Parents, my brothers, and my sisters for their love and support.

Sabah Ramadhan Mohammed

20 July, 2019

TABLE OF CONTENTS

	Page
ACKNOWLEDGEMENT	ii
TABLE OF CONTENTS	iii
LIST OF TABLES	vi
LIST OF FIGURES	vii
LIST OF SYMBOLS	xv
LIST OF ABBREVIATIONS	xix
ABSTRAK	xxi
ABSTRACT	xxiii
CHAPTER 1 INTRODUCTION	1
1.1 Background	1
1.2 Problem Statement	9
1.3 Objectives	11
1.4 Scope of the Thesis	11
1.5 Thesis Structure	12
CHAPTER 2 LITERATURE REVIEW	13
2.1 Overview	13
2.2 The Performance Comparison of Existing AC and DC Systems	13
2.3 Main Components of an HVDC Power System	18
2.3.1 12-Pulse HVDC Converter Unit	18
2.3.2 HVDC Transmission Medium	24
2.3.3 HVDC Electrode	27
2.4 Impacts of HVDC Ground/Sea Electrodes	34
2.4.1 Impact of the Corrosion on Metallic Objects	34

2.4.2	Impact of Ground/Return Current on an AC Power Transformers	40
2.4.3	Impacts of HVDC Ground/Sea Electrode on the Environment	43
2.5	The Topology of Existing LCC-HVDC Systems and Operating Modes	47
2.5.1	BTBS Topology	48
2.5.2	1PS Topology	49
2.5.3	2PS Topology	50
2.5.4	Multi-pole System	55
2.6	Summary	58
CHAPTER 3 METHODOLOGY		59
3.1	Introduction	59
3.2	Operational Concepts of the Proposed 4PS	59
3.2.1	System Topology and its Operating Modes	59
3.2.2	Power Capacity and Power Losses	63
3.2.3	The Size of the Conductor Required	67
3.2.4	Transmission Power Density	69
3.2.5	Reliability Evaluation Model for Whole System	72
3.3	Simulation Verification	78
3.3.1	System Description	78
3.3.2	Control and Protection Subsystem Description	82
3.4	Experimental Verification	83
3.4.1	Experimental Setup	83
3.4.1 (a)	Design of the Proposed 4PS	85
3.4.1 (b)	The Conventional 2PS	87
3.4.2	Equipment and Tools	89
3.4.3	Design and Implementation of a Special Transformer	90
3.5	Summary	94
CHAPTER 4 RESULTS AND DISCUSSION		95

4.1	Introduction	95
4.2	Mathematical Analysis and Results	96
4.2.1	Comparison of Results Between 2PS and 4PS Topologies	96
4.2.2	The Contributions of the Proposed 4PS in an HVDC System	97
4.3	Simulation Results	98
4.3.1	Normal Mode Operation	98
4.3.1 (a)	The 2PS During Normal Mode Operation	98
4.3.1 (b)	The Proposed 4PS During Normal Mode Operation	104
4.3.2	Mono-pole and Bi-pole in Failure Mode Operations	108
4.3.2 (a)	Mono-pole Failure in the Conventional 2PS	109
4.3.2 (b)	Bi-pole Failure in the Proposed 4PS	113
4.3.3	AC Line-to-Ground Fault at the Inverter Side	117
4.3.4	Total Harmonic Distortion of the AC Line Currents	124
4.3.5	Comparison Between the 2PS and 4PS Simulation Results	128
4.4	Experimental Results	129
4.4.1	The Conventional 2PS at Normal Mode Operation	130
4.4.2	The Proposed 4PS at Normal Mode Operation	133
4.4.3	The 2PS and 4PS at Failure Mode Operation	136
4.4.4	THD of the AC Currents for 2PS and 4PS	140
4.5	Comparison Between the 2PS and 4PS Experimental Results	141
4.6	Summary	142
CHAPTER 5 CONCLUSION AND FUTURE RECOMMENDATIONS ..		144
5.1	Conclusion	144
5.2	Recommendations for Future Research	146
REFERENCES.....		147

LIST OF PUBLICATIONS

LIST OF TABLES

		Page
Table 2.1	Types of HVDC Electrodes	27
Table 2.2	Parameters of Toroidal Grounding Electrode (Chen <i>et al.</i> , 2008)	46
Table 2.3	Operating Modes of the Existing 2PS	50
Table 2.4	Operating Modes of ± 800 kV 2PS LCC Ultra HVDC Transmission	53
Table 3.1	Operating Modes of the Proposed 4PS	60
Table 3.2	2PS and 4PS Parameters for the Simulation Model	79
Table 3.3	Master Control Modification for the Proposed 4PS	82
Table 3.4	2PS and 4PS Parameters for the Laboratory Prototype	88
Table 3.5	General description for the Laboratory Prototype Equipment	89
Table 3.6	The Parameters of the Transformer Prototype Design	93
Table 4.1	Comparison of Results for the 2PS and 4PS Topologies	96
Table 4.2	Harmonic Order and THD of Phase <i>a</i> Current Waveform Simulation Results for 2PS and 4PS	127
Table 4.3	Comparison of the AC Powers, Losses, system topology and THD between 2PS and 4PS Simulation Results	128
Table 4.4	Comparison Between the 2PS and 4PS Experimental Results	142

LIST OF FIGURES

	Page
Figure 2.1	The power transfer mechanism of (a) the AC line and (b) DC line 15
Figure 2.2	(a) capacitive characteristics of AC cable, (b) inductive characteristics of AC overhead line, (c) transmission capacity of AC and DC systems with underground cables, and (d) with overhead lines (Claes <i>et al.</i> , 2014). 17
Figure 2.3	The loadability characteristics of the three-phase double-circuit AC system ($2 \times 3PL$) versus 2PS HVDC system ($2 \times DCL$) (Lauria <i>et al.</i> , 2014b). 17
Figure 2.4	LCC HVDC system (a) Main Components, (b) 12-pulse HVDC converter unit, (c) Thyristor valve, and (d) arrangements of the transformer 20
Figure 2.5	Voltage and current waveforms of a 12-pulse HVDC converter unit: (a) DC voltage waveform, (b) AC current waveform with harmonics (Kim <i>et al.</i> , 2009). 22
Figure 2.6	Variation of reactive power with active power (Arrilaga <i>et al.</i> , 2007). 23
Figure 2.7	Structure of ± 500 kV DC tower of the Three Gorges-Shanghai HVDC transmission (Lui and Dinavahi, 2018). 25
Figure 2.8	Cross-section of a 500 MW and 350 kV mass-impregnated submarine HVDC cable (Arrilaga <i>et al.</i> , 2007). 26
Figure 2.9	(a) Land electrode ring arrangement, (b) Manitoba bipole 1 project, Canada, at Radisson converter with land electrode (Hu <i>et al.</i> , 2014). 28
Figure 2.10	Vertical land electrode of Yunnan-Guangdong project at converter station 1 (Hu <i>et al.</i> , 2014). 29
Figure 2.11	Deep well electrode of Guizhou-Guangdong II project at Guizhou converter (Hu <i>et al.</i> , 2014). 30

Figure 2.12	Beach electrode of Skagerrak multi-pole HVDC link project at Norway converter (Hu <i>et al.</i> , 2014).	31
Figure 2.13	Pond shore electrode of Gotlan HVDC link project at Sweden mainland converter (Hu <i>et al.</i> , 2014).	32
Figure 2.14	Sea electrode of Kontek HVDC link at Denmark converter (Hu <i>et al.</i> , 2014).	33
Figure 2.15	(a) A 355.6 mm × 9.53 mm API 5L X52 steel pipes: (b) and (c) time dependence of the potential of API 5L X52 steel electrode in the anodic and cathodic zones, respectively, at various DC current densities in the soil solution; (d) optical views of the morphology of steel electrodes with different DC current densities (Qian and Cheng, 2017).	36
Figure 2.16	Impact of the corrosion on the suspension insulator: (a) Principle of the electrolytic corrosion of iron part, (b) Influence of corrosion on the pin, (c) Failure form of pin corroded insulator (Luo <i>et al.</i> , 2016).	39
Figure 2.17	Overview of AC system exposed to a field from HVDC electrode (Hu <i>et al.</i> , 2014).	41
Figure 2.18	Waveforms of magnetic strength for a power transformer under DC bias at various DC current: (a) Limb phases A and C, (b) Limb phase B, (c) Side limb (Li <i>et al.</i> , 2010).	42
Figure 2.19	Step voltage due to an HVDC electrode (Mukhedkar and Dawalibi, 1983; Kamakshaiah and Kamaraju, 2011).	44
Figure 2.20	A sample grounding electrode spatial temperature distribution in the Y-X plane of the soil (Chen <i>et al.</i> , 2008).	46
Figure 2.21	Topology for existing LCC-HVDC Systems : (a) 1PBTBS, (b) 2PBTBS, (c) 1PS, (d) 2PS (IEEE Std 1030, 1987; Zehong, 2011)	47
Figure 2.22	Switching arrangement for operating a 2PS in metallic return mode (Kamakshaiah and Kamaraju, 2011).	52
Figure 2.23	Single Line Figure of a Typical ±800 kV 2PS Ultra LCC-HVDC Transmission System (Xie <i>et al.</i> , 2016).	53
Figure 2.24	Itaipu HVDC Transmission System with Two a Common Electrode (Groham, 2005; Praca <i>et al.</i> , 1996).	56

Figure 2.25	Skagerrak HVDC transmission system with a common sea electrode (Andersson <i>et al.</i> , 2015).	57
Figure 3.1	The proposed 4PS Topology	60
Figure 3.2	Equivalent circuit of LCC HVDC transmission topology, (a) conventional 2PS, (b) proposed 4PS	61
Figure 3.3	Overhead transmission conductors arranged uniformly around circles, (a) existing 2PS with radius $r_{2ps} = d$, (b) proposed 4PS with radius $r_{4ps} = d/\sqrt{2}$	71
Figure 3.4	Reliability logic diagram of, (a) conventional 2PS, (b) proposed 4PS	73
Figure 3.5	Monopolar Outages in the existing 2PS (Grey color), (a) Pole 1 outage, (b) Pole 2 outage	74
Figure 3.6	Bipolar Outages in the proposed 4PS (Grey color), (a) Poles 1 & 2 outage, (b) Poles 2 & 3 outage, (c) Poles 3 & 4 outage, (d) Poles 4 & 1 outage	75
Figure 3.7	Transmission capacity of, (a) existing 2PS topology, (b) proposed 4PS topology	76
Figure 3.8	Simulation model of the 2PS in MATLAB/SIMULINK	80
Figure 3.9	Simulation model of the 4PS in MATLAB/SIMULINK	81
Figure 3.10	Hardware Photograph of the Laboratory Prototype	85
Figure 3.11	Schematic Diagram of the Proposed 4PS Setup	86
Figure 3.12	Schematic Diagram of the Conventional 2PS	87
Figure 3.13	Implementation of the transformer prototype, (a) hardware photograph, (b) and (c) construction and dimensions, and (d) windings arrangement	92
Figure 4.1	Waveforms for 2PS at normal state operation: (a) DC voltage at each six-pulse rectifier bridge, (b) line-to-ground DC voltages at rectifier side, (c) DC line currents at rectifier side, (d) alpha degrees for rectifier bridges, (e) DC voltage at each six-pulse inverter bridge, (f) line-to-ground DC voltages at inverter side, (g) DC line currents at inverter side, (h) alpha degrees for inverter bridges	99
Figure 4.2	Waveforms for 2PS at normal state operation: (a) pole-to-ground DC current faults, (b) line-to-ground AC voltages at system 1, (c)	

	AC line currents at system 1, (d) active and reactive powers at AC system 1, (e) pole-to-ground AC current fault, (f) line-to-ground AC voltages at system 2, (g) AC line currents at system 2, (h) active and reactive powers at AC system 2 101
Figure 4.3	Waveforms for 2PS at normal state operation: (a) line-to-line voltages V_{ab} at each secondary transformer for rectifier side, (b) phase currents i_a at each secondary transformer for rectifier side, (c) valve voltages (valve 1) for each rectifier bridge, (d) valve currents (valve 1) for each rectifier bridge, (e) line-to-line voltages V_{ab} at each secondary transformer for inverter side, (f) phase currents i_a at each secondary transformer for inverter side, (g) valve voltages (valve 1) for each inverter bridge, (h) valve currents (valve 1) for each inverter bridge 103
Figure 4.4	Waveforms for 4PS at normal state operation: (a) DC voltage at each six-pulse rectifier bridge, (b) line-to-line DC voltages at rectifier side, (c) DC line currents at rectifier side, (d) alpha degrees for rectifier bridges, (e) DC voltage at each six-pulse inverter bridge, (f) line-to-line DC voltages at inverter side, (g) DC line currents at inverter side, (h) alpha degrees for inverter bridges 105
Figure 4.5	Waveforms for 4PS at normal state operation: (a) pole-to-ground DC current faults, (b) line-to-ground AC voltages at system 1, (c) AC line currents at system 1, (d) active and reactive powers at AC system 1, (e) pole-to-ground current AC fault, (f) line-to-ground AC voltages at system 2, (g) AC line currents at system 2, (h) active and reactive powers at AC system 2 106
Figure 4.6	Waveforms for 4PS at normal mode operation: (a) line-to-line voltages V_{ab} at each secondary transformer for rectifier side, (b) phase currents i_a at each secondary transformer for rectifier side, (c) valve voltages (valve 1) for each rectifier bridge, (d) valve currents (valve 1) for each rectifier bridge, (e) line-to-line voltages V_{ab} at each secondary transformer for inverter side, (f) phase currents i_a at each secondary transformer for inverter side, (g) valve voltages (valve 1) for each inverter bridge, (h) valve currents (valve 1) for each inverter bridge 107

Figure 4.7	Waveforms for 2PS at mono-pole failure mode operation: (a) pole-to-ground DC current faults, (b) line-to-ground AC voltages at system 1, (c) AC line currents at system 1, (d) active and reactive powers at AC system 1, (e) pole-to-ground AC current fault, (f) line-to-ground AC voltages at system 2, (g) AC line currents at system 2, (h) active and reactive powers at AC system 2 110
Figure 4.8	Waveforms for 2PS at mono-pole failure mode: (a) DC voltage at each six-pule rectifier bridge, (b) line-to-ground DC voltages at rectifier side, (c) DC line currents at rectifier side, (d) alpha degrees for rectifier bridges, (e) DC voltage at each six-pulse inverter bridge, (f) line-to-ground DC voltages at inverter side, (g) DC line currents at inverter side, (h) alpha degrees for inverter bridges 111
Figure 4.9	Waveforms for 2PS at mono-pole failure mode: (a) line-to-line voltages V_{ab} at each secondary transformer for rectifier side, (b) phase currents i_a at each secondary transformer for rectifier side, (c) valve voltages (valve 1) for each rectifier bridge, (d) valve currents (valve 1) for each rectifier bridge, (e) line-to-line voltages V_{ab} at each secondary transformer for inverter side, (f) phase currents i_a at each secondary transformer for inverter side, (g) valve voltages (valve 1) for each inverter bridge, (h) valve currents (valve 1) for each inverter bridge 112
Figure 4.10	Waveforms for 4PS at bi-pole failure mode operation: (a) pole-to-ground DC current faults, (b) line-to-ground AC voltages at system 1, (c) AC line currents at system 1, (d) active and reactive powers at AC system 1, (e) pole-to-ground AC current fault, (f) line-to-ground AC voltages at system 2, (g) AC line currents at system 2, (h) active and reactive powers at AC system 2 114
Figure 4.11	Waveforms for 4PS at bi-pole failure mode: (a) DC voltage at each six-pulse rectifier bridge, (b) line-to-ground DC voltages at rectifier side, (c) DC line currents at rectifier side, (d) alpha degrees for rectifier bridges, (e) DC voltage at each six-pulse inverter bridge, (f) line-to-ground DC voltages at inverter side, (g) DC line currents at inverter side, (h) alpha degrees for inverter bridges 115

Figure 4.12	Waveforms for 4PS at bi-pole failure mode: (a) line-to-line voltages V_{ab} at each secondary transformer for rectifier side, (b) phase currents i_a at each secondary transformer for rectifier side, (c) valve voltages (valve 1) for each rectifier bridge, (d) valve currents (valve 1) for each rectifier bridge, (e) line-to-line voltages V_{ab} at each secondary transformer for inverter side, (f) phase currents i_a at each secondary transformer for inverter side, (g) valve voltages (valve 1) for each inverter bridge, (h) valve currents (valve 1) for each inverter bridge	116
Figure 4.13	Waveforms for the conventional 2PS at AC line-to-ground fault at the inverter side: (a) pole-to-ground DC current faults, (b) line-to-ground AC voltages at system 1, (c) AC line currents at system 1, (d) active and reactive powers at AC system 1, (e) pole-to-ground AC current fault, (f) line-to-ground AC voltages at system 2, (g) AC line currents at system 2, (h) active and reactive powers at AC system 2	119
Figure 4.14	Waveforms for the conventional 2PS at AC line-to-ground fault at the inverter side: (a) DC voltage at each six-pulse rectifier bridge, (b) line-to-ground DC voltages at rectifier side, (c) DC line currents at rectifier side, (d) alpha degrees for rectifier bridges, (e) DC voltage at each six-pulse inverter bridge, (f) line-to-ground DC voltages at inverter side, (g) DC line currents at inverter side, (h) alpha degrees for inverter bridges	120
Figure 4.15	Waveforms for the conventional 2PS at AC line-to-ground fault at the inverter side: (a) line-to-line voltages V_{ab} at each secondary transformer for rectifier side, (b) phase currents i_a at each secondary transformer for rectifier side, (c) valve voltages (valve 1) for each rectifier bridge, (d) valve currents (valve 1) for each rectifier bridge, (e) line-to-line voltages V_{ab} at each secondary transformer for inverter side, (f) phase currents i_a at each secondary transformer for inverter side, (g) valve voltages (valve 1) for each inverter bridge, (h) valve currents (valve 1) for each inverter bridge	121

Figure 4.16	Waveforms for the proposed 4PS at AC line-to-ground fault at the inverter side: (a) pole-to-ground DC current faults, (b) line-to-ground AC voltages at system 1, (c) AC line currents at system 1, (d) active and reactive powers at AC system 1, (e) pole-to-ground AC current fault, (f) line-to-ground AC voltages at system 2, (g) AC line currents at system 2, (h) active and reactive powers at AC system 2	122
Figure 4.17	Waveforms for the proposed 4PS at AC line-to-ground fault at the inverter side: (a) DC volyage at each six-pulse rectifier bridge, (b) line-to-ground DC voltages at rectifier side, (c) DC line currents at rectifier side, (d) alpha degrees for rectifier bridges, (e) DC volyage at each six-pulse inverter bridge, (f) line-to-ground DC voltages at inverter side, (g) DC line currents at inverter side, (h) alpha degrees for inverter bridges	123
Figure 4.18	Waveforms for the proposed 4PS at AC line-to-ground fault at the inverter side: (a) line-to-line voltages V_{ab} at each secondary transformer for rectifier side, (b) phase currents i_a at each secondary transformer for rectifier side, (c) valve voltages (valve 1) for each rectifier bridge, (d) valve currents (valve 1) for each rectifier bridge, (e) line-to-line voltages V_{ab} at each secondary transformer for inverter side, (f) phase currents i_a at each secondary transformer for inverter side, (g) valve voltages (valve 1) for each inverter bridge, (h) valve currents (valve 1) for each inverter bridge	124
Figure 4.19	Phase a current waveforms of the conventional 2PS and the proposed 4PS: (a) Phase a current waveforms of the primary winding at each transformer on the rectifier side in the 2PS, (b) Phase a current waveform on the AC system 1 in the 2PS, (c) Phase a current waveforms of the primary winding at each transformer on the inverter side in the 2PS, (d) Phase a current waveform on the AC system 2 in the 2PS, (e) Phase a current waveforms of the primary winding at each transformer on the rectifier side in the 4PS, (f) Phase a current waveform on the AC system 1 in the 4PS,	

	(g) Phase a current waveforms of the primary winding at each transformer on the inverter side in the 4PS, (h) Phase a current waveform on the AC system 2 in the 4PS	126
Figure 4.20	Voltage waveforms for 2PS: (a) line-to-ground AC voltages at the primary winding, (b) line-to-line AC voltages V_{ab} at each secondary winding, (c) line-to-ground DC voltages with 12-pulse harmonic	131
Figure 4.21	Current waveforms for 2PS: (a) line AC currents at primary winding, (b) line AC currents i_a at each secondary winding, (c) DC line currents	132
Figure 4.22	Voltage waveforms for 4PS: (a) line-to-ground AC voltages at the primary winding, (b) line-to-line AC voltages V_{ab} at each secondary winding, (c) line-to-ground DC voltages with 12-pulse harmonic	134
Figure 4.23	Current waveforms for 4PS: (a) line AC currents at primary winding, (b) line AC currents i_a at each secondary winding, (c) DC line currents	135
Figure 4.24	Voltage and current waveforms for 2PS: (a) line AC currents at primary winding, (b) line AC currents i_a at each secondary winding, (c) line-to-ground DC voltage with 12-pulse harmonic, (d) DC line currents	138
Figure 4.25	Voltage and current waveforms for 4PS: (a) line AC currents at primary winding, (b) line AC currents i_a at each secondary winding, (c) line-to-line DC voltage with 12-pulse harmonic, (d) DC line currents	139
Figure 4.26	THD of the current phases a, b, c waveforms at primary winding transformer: (a) conventional 2PS, (b) proposed 4PS	140

LIST OF SYMBOLS

\emptyset	Power factor angle
α	Thyristor firing angle
α_R	Firing angle of the rectifier
α_I	Firing angle of the inverter
V_p	Peak value of the AC voltage
V_{rms}	RMS value of the AC voltage
V_{LL}	Line-to-line AC voltage (in rms)
V_d	DC voltage
i_p	Peak value of the AC line current
i_{rms}	RMS value of the AC line current
i_d	DC line current
i_1, i_2, i_3, i_4	DC current of loop 1, 2, 3, 4 in the 4PS, respectively
i_{2PS}	DC line currents for 2PS
i_{4PS}	DC line currents for 4PS
R_{ac}	Resistance of the AC conductor
R_{dc}	Resistance of the DC conductor
R_{2PS}	Resistance of the DC conductor for 2PS
R_{4PS}	Resistance of the DC conductor for 4PS
P_{ac}	AC Power
P_{dc}	DC Power
P_{2PS}	Total DC power transmitted by the conventional 2PS
P_{4PS}	Total DC power transmitted by the proposed 4PS
P_1, P_2	DC powers transmitted by circuit 1, 2 in the 2PS, respectively
P_1, P_2, P_3, P_4	DC powers transmitted by circuit 1, 2, 3, 4 in the 4PS, respectively

W_{ac}	Power losses in AC conductor
W_{dc}	Power losses in DC conductor
W_{2PS}	Total power losses by two-HVDC line in the 2PS
W_{4PS}	Total power losses by four-HVDC line in the 4PS
ω	$\omega = 2\pi f$
f	Fundamental system frequency
$V_{d,R}$	DC terminal voltage of the six-pulse rectifier bridge
$V_{d,I}$	DC terminal voltage of the six-pulse inverter bridge
A_{2PS}	Cross-sectional area of the conductor in square meters for 2PS
A_{4PS}	Cross-sectional area of the conductor in square meters for 4PS
D_{2PS}	Density of power transmission in a unit space radius for 2PS
D_{4PS}	Density of power transmission in a unit space radius for 4PS
r	The radius of the circle in meter
r_{2PS}	Radius for 2PS transmission lines arrangement
r_{4PS}	Radius for 4PS transmission lines arrangement
d	The distance unit between two conductors
$3L_R$	Three-phase transformer inductance at rectifier side
$3L_I$	Three-phase transformer inductance at inverter side
P	Active power
Q	Reactive power
kV	Kilo Volt
kN	Kilo Newton
V_L	Inductance voltage
i_c	Capacitance current
MW	Megawatts
T	Temperature [$^{\circ}C$]

e_{th}	Thermal Energy [j/m^3]
ρ	Resistivity of Material [$\Omega \cdot m$]
E	Electric Field Strength [V/m]
t	Time in second [s]
m	The soil mass in [kg]
c_s	The specific heat capacity [$j/kg \text{ }^\circ\text{C}$]
j	Joule (Energy unit)
J	Current density [A/m^2]
p	Pulse number
k	Integer
Y_g/Y	Wye-grounded/wye transformer connection
Y_g/D	Wye-grounded/delta transformer connection
V_{in}	Transformer AC voltage input
V_{out}	Transformer AC voltage output
N_{pri}	Number of the primary winding turns
N_{sec}	Number of the secondary winding turns
Φ_m	Magnetic flux (in <i>Weber</i>)
x	Reactance
Z	Impedance
X_L	Pure inductance
$\sin \delta$	Phase angle between sending end and receiving end voltages
H	Magnetic field strength
B	Flux density (Tesla)
A_c	Cross-sectional area of the transformer core (in mm^2)
A_s	Cross-sectional area of the transformer slot (in mm^2)
A	Cross-sectional area of the wire in special transformer (in mm^2)

h Harmonic order

C_{2PS}, C_{4PS} Available capacities for 2PS and 4PS, respectively.

LIST OF ABBREVIATIONS

AAAC	All Aluminum Alloy Conductor
ABB	Asia Brown Boveri Ltd.
ACCC	Aluminum Conductor Composite Core
AC	Alternating Current
ACCR	Aluminum Conductor Composite Reinforced
ACSR	Aluminum Conductor Steel Reinforced
BTBS	Back-to-Back System
CB	Circuit Breaker
CCC	Capacitor Commutated Converters
CIGRE	International Council on Large Electric Systems
CSE	Copper/ Copper Sulfate Reference Electrode
DC	Direct Current
EPRI	Electric Power Research Institute
GTO	Gate Turn-Off Thyristor
HVAC	High Voltage Alternating Current
HVDC	High Voltage Direct Current
IEC	The International Electrotechnical Commission
IEEE	The Institute of Electrical and Electronics Engineers
IGBT	Insulated Gate Bipolar Transistor
LCC	Line Commutated Converter
MPS	Multi-Pole System
MRTB	Metallic Return Transfer Breaker
NACE	National Association of Corrosion Engineers
NBD	Neutral Blocking Device

OCSC	Overall Cumulative Size of Conductors
PWM	Pulse Width Modulation
ROW	Right-of-Way
SCR	Short Circuit Ratio
SR	Smoothing Reactor
THD	Total Harmonic Distortion
VSC	Voltage Source Converter
XLPE	Cross Linked Polyethylene
1PBTBS	One-Pole Back-to-Back System
2PBTBS	Two-Pole Back-to-Back System
1PS	Mono-pole System
2PS	Bi-pole System
4PS	Four-Pole System

TOPOLOGI DIPERBAIKI BAGI PENUKAR PENUKARTERTIB-TALIAN HVDC DENGAN SISTEM EMPAT KUTUB

ABSTRAK

Elektrod bumi/laut atau logam palangan adalah bahagian penting dalam sistem sedia ada penghantaran kuasa arus terus voltan tinggi (HVDC) untuk arus pulangan. Di samping kewujudan elektrod bumi/laut atau kepingan pulangan logam yang mahal dalam topologi HVDC konvensional, elektrod bumi/laut menghasilkan kesan buruk yang teruk terhadap alam sekitar dan sistem kuasa arus ulang-alik (AC) berdekatan (kakisan struktur metalik yang dikebumikan, kepanasan melampau tanah/air, DC pincang dalam pengubah kuasa, dan sebagainya). Tesis ini mencadangkan kebaharuan sistem empat kutub (4PS) untuk penghantaran penukar penukartertib-talian (LCC) HVDC. Sistem ini bertujuan untuk menghapuskan penggunaan elektrod bumi/laut atau logam pulangan dan meningkatkan kebolehpercayaan dan ketumpatan penghantaran kuasa. Cadangan prinsip operasi sistem ini dibentangkan, diikuti dengan analisa matematik terperinci bagi sistem bipolar konvensional (2PS) dan 4PS yang dicadangkan. Keputusan matematik menunjukkan bahawa kuasa elektrik boleh dipindahkan melalui empat litar DC selari yang berkesan dengan operasi 12-nadi dalam 4PS dan bukannya hanya dua litar DC dengan operasi 12-nadi seperti dalam 2PS yang sedia ada. Tambahan pula, di bawah kapasiti kuasa yang sama yang dihantar dalam kedua-dua sistem 2PS dan 4PS, hasilnya menunjukkan peningkatan kebolehpercayaan sistem dan ketumpatan penghantaran kuasa 4PS kira-kira 2 dan $\sqrt{2}$ kali, masing-masing, berbanding dengan 2PS. Di samping itu, keputusan simulasi Penyelewengan Harmonik Jumlah (THD) dari arus AC bertambah baik dalam novel 4PS sebanyak 2.12% pada sistem AC 1 dan 0.89% pada sistem AC 2 berbanding

dengan 2PS konvensional. Prestasi sistem yang dicadangkan telah disahkan oleh hasil simulasi dan ujikaji. Hasil simulasi dan ujikaji menunjukkan bahawa topologi 4PS yang dicadangkan boleh menghapuskan elektrod bumi atau pulangan logam, menghasilkan empat litar DC selari yang berkesan dengan operasi 12-nadi dan meningkatkan keboleharapan dan ketumpatan kuasa.

IMPROVED TOPOLOGY FOR LINE-COMMUTATED CONVERTER HVDC WITH FOUR-POLE SYSTEM

ABSTRACT

The ground/sea electrode or metallic return is an essential part of the existing high-voltage direct current (HVDC) power transmission systems for carrying its return current. Besides the costly presence of the ground/sea electrode or metallic return in the conventional HVDC topologies, the ground/sea electrode is producing severe adverse effects on the environment and alternating current (AC) power systems nearby (e.g. corrosion of buried metallic structures, soil/water overheating, DC bias in power transformers, etc.). This thesis proposes a novel four-pole system (4PS) for line-commutated converter (LCC) HVDC transmission. This system aims to eliminate ground/sea electrode or metallic return and increase the reliability and density of power transmission. The operating principles of the proposed system are presented, followed by detailed mathematical analysis of the conventional bi-pole system (2PS) and the proposed 4PS. Mathematical results show that the electrical power can be transferred through four effective parallel DC circuits with the 12-pulse operation in the 4PS instead of only two DC circuits with the 12-pulse operation as in the existing 2PS. Furthermore, under the same power capacity transmitted in both systems 2PS and 4PS, the results show an increase in system reliability and power transmission density of the 4PS approximately 2 and $\sqrt{2}$ times, respectively, in comparison with the 2PS. In addition, the Total Harmonic Distortion (THD) simulation results of the AC currents improved in a novel 4PS by 2.12 % at AC system 1 and 0.89 % at AC system 2 in comparison with the conventional 2PS. The proposed system performance has been verified by simulation and experimental results. Simulation and experimental results

showed that the proposed 4PS topology can eliminate ground electrode or metallic return, produce four effective parallel DC circuits with 12-pulse operation and increase the reliability and power density.

CHAPTER 1

INTRODUCTION

1.1 Background

In the early 1880s, the first commercial electricity generated, transmitted, and distributed by Thomas Edison was a Direct Current (DC) electrical power system. This system had DC generators driven by steam engines and supplying DC power at 110 V through underground cables to an area of about 1.6 km radius (Kamakshaiah and Kamaraju, 2011). The drawback of Edison's system is difficulty in obtaining the necessary DC voltage levels required for transmitting electrical power over a long distance with low line losses (Rudervall *et al.*, 2000). Generally, in a DC power system, neither DC voltage can be stepped up nor DC power can be generated at high voltage (Lucas, 2001). In the late 1880s, the three-phase Alternating Current (AC) electrical power system by Nikola Tesla made it possible to easily stepped up the voltage levels at high voltage to minimize the transmission losses (Setreus and Bertling, 2008). In Tesla's system, at sending end of the transmission line, the voltage level is stepped up by means of step-up transformers to the required value for transmission of electric power over long distances. At receiving end the voltage level is stepped down by means of step-down transformers for distribution purpose (Kishore and Singal, 2014). Because this efficient mechanism, the AC system has been the dominating technology for electrical power system ever since (Pierri *et al.*, 2017).

The major constraint of the conventional High Voltage Alternating Current (HVAC) systems is the presence of large inductance that causes phase shifts between the voltage and current waveforms (power factor angle) which limits to the transmission capacity (Arrilaga *et al.*, 2007). Inductance can introduce severe adverse effects in an AC system. These adverse effects include the stability problem, which is

that the voltage phase angle between the sending end and receiving end should not exceed 30 degrees at full-load for transient stability (Kalair *et al.*, 2016). Limitation of AC line length is the next effect. If the AC line length is more than 500 km, reactive power generated by the HVAC line is greater than its power transmitting capacity (Kamakshaiah and Kamaraju, 2011). Thus, the maximum permissible line length in HVAC transmission systems is 500 km (Lucas, 2001). A recent study (Kalair *et al.*, 2016) address that the HVAC cables and overhead lines remain economical only up to 50 km and 600 km, respectively. Whereas, with reactive power compensation equipment, the HVAC overhead line length extended to 1000 km and this equipment add cost to the HVAC system (Lucas, 2001). The skin effect of AC current is another adverse effect, which is the AC current flows only through the outer part of the conductor, therefore, the whole cross-section area of the conductor is not used (Farzaneh *et al.*, 2012). Another disadvantage of AC systems is that the interconnection between AC power systems must be synchronous. Thus, the main drawback of AC systems is the different frequency power systems cannot be interconnected (Abu-Rub *et al.*, 2014). By contrast, in the DC systems, the frequency is zero, hence the inductance and capacitance parameters do not limit the transmission capacity or the maximum length of a DC overhead line or cable (Siemens, 2011). Furthermore, the cross-section area of the DC conductor is fully utilized, thus, for the same size of the conductor, the DC system can carry greater power in comparison with the AC system (Rudervall *et al.*, 2000). The voltage level in the DC system can be designed equivalent to the peak value of the voltage level in the AC system. Thus, for the same amount of insulation between line voltage and ground, the ratio of DC voltage to the peak AC voltage is $\sqrt{2}$ (Weedy *et al.*, 2012; Lucas, 2001).

High Voltage Direct Current (HVDC) technology has characteristics that make it alternative for the existing HVAC power systems (Kalair *et al.*, 2016). The basic principle that occurs in modern HVDC system is transferring electric energy from one AC system to a second AC system and vice versa via the HVDC link (Andersen, 2006). For this purpose, the modern HVDC system consists of two converter stations at each end of the HVDC link (Kim *et al.*, 2009). For example, in 1954 Gotland scheme in Sweden was the first commercial HVDC transmission system with voltage 100 kV and the capacity of 20 MW over 98 km long submarine cable. In this scheme, Mercury Arc Valves were used for converting electric energy from AC to DC at the sending end and converting back the DC to AC at the receiving end (Sakai *et al.*, 2014). Since 1970, the thyristor has been developed for carrying high voltage and large current efficiently, so far the thyristor ratings of over 8kV and 4kA. By connecting the thyristor devices in series, it is possible to build up a thyristor valve. This modular structure permits the use of thyristor valves of any power and voltage rating (Kim *et al.*, 2009). For example, the DC voltage test results meet the requirements of ± 800 kV thyristor valve (Huang *et al.*, 2009). Undoubtedly, with the development of HVDC converters based on thyristor valves, it was possible to once again transmit bulk DC power at high voltages and over long distances, giving rise to HVDC systems (Kim *et al.*, 2009). The advantage and disadvantage of modern HVDC over a conventional HVAC transmission systems are the 12-pulse HVDC converter units of an HVDC system are more expensive than HVAC stations but the transmission lines of the HVDC lines are cheaper (Weedy *et al.*, 2012). The cost of 12-pulse HVDC converters are 36% of HVDC system cost structure (Rudervall *et al.*, 2000). For the same amount of electric power transmitting, the costs and losses of an HVDC transmission become lower than an HVAC if the transmission distance exceeded certain threshold usually

referred to as the “breakeven-distance”, which is approximately 800 *km* for overhead line and 50 *km* for submarine or underground cable (Weedy *et al.*, 2012).

HVDC system is now available in two basic converter technologies: Line Commutated Converter (LCC) and Voltage Source Converter (VSC). Both technologies are used for converting electrical energy from AC to DC or vice versa (Pierri *et al.*, 2017). The conventional HVDC based on LCC technology employing thyristor valves for converting AC-power to DC-power and vice versa. This technology was introduced in the late 1960s (Bahrman and Johnson, 2007). The LCC is a constant current source converter and operated only at AC system voltage frequency with 50 or 60 *Hz* for commutation (Rudervall *et al.*, 2000). Commutation is the transfer of current from one phase to another in a synchronized firing sequence of the thyristor valves (Bahrman and Johnson, 2007). As a result, the AC phase current always lags the phase voltage and the LCC converters consume reactive power approximately between 50% to 60% of the transmitted DC power (Kim *et al.*, 2009; Bakas *et al.*, 2017; Huang *et al.*, 2009; Sellick and Åkerberg, 2012; Siyu *et al.*, 2012). This blocks the connection of LCC-HVDC system to a weak AC system because of the risk of inverter commutation failures when connected to a weak AC system (Arrilaga *et al.*, 2007). For this reason, the Short Circuit Ratio (SCR) of the AC grids should be at least twice or more (Kim *et al.*, 2009). According to the IEEE standard (IEEE Std 1204-1997), the SCR is the ratio of the three-phase short-circuit of the AC system (*MVA*) to the power rating of the DC system (*MW*) (Krishayya *et al.*, 1997). In the late 1990s, this drawback has been avoided in recent LCC systems by deploying the Capacitor Commutated Converters (CCC) concept, which is the use of commutation capacitors inserted in series between the converter transformers and the thyristor valves (Rudervall *et al.*, 2000). Since the 1960s, LCC conversion technology

has been used in the majority of the HVDC systems in the world for bulk power transmission over long distance and interconnection of two AC power systems with different frequencies (Pierri *et al.*, 2017; Transmission, 2012; Kumar *et al.*, 2006).

The second technology that used for electrical energy conversion is HVDC system based on VSC which is employing Insulated Gate Bipolar Transistor (IGBT) or Gate Turn-Off Thyristor (GTO) valves (Vural, 2016). This technology was introduced in the late 1990s (Bahrman and Johnson, 2007). The VSC is a constant voltage source converter and operating with Pulse Width Modulation (PWM) at high frequency (not with the AC system frequency as in the LCC) (Adam and Williams, 2016). The main advantages of this technology are the possibility to control both active and reactive power independently and no restriction on the minimum SCR of the AC grids (Bahrman and Johnson, 2007). Although the VSC-HVDC system presents a competitive alternative to the LCC-HVDC system, this technology suffers from high switching losses (Jung *et al.*, 2017). According to the study results (Arrilaga *et al.*, 2007), the energy loss by frequency used for the switching of the valves IGBT-based VSC (two-level with a PWM frequency of 1950 Hz), IGBT-based VSC (three-level with a PWM frequency of 1260 Hz), and thyristor-based LCC were 3%, 1.8%, and 0.8%, respectively. According to the report (Andersen, 2006), the efficiency of 12-pulse HVDC converter unit based on LCC was about 99.3%. Whereas, the efficiency of VSC-HVDC converter unit was around 98.2%. Thus, with high power applications, the switching losses in the VSC-HVDC systems are one of the challenging issues that need to be handled. Presently, the power and voltage ratings of VSC-HVDC is very much lower than LCC-HVDC systems (Weedy *et al.*, 2012).

According to the IEEE standard (IEEE Std 1378, 1997), the 12-pulse HVDC converter unit consists of two, fully controlled, six-pulse bridges connected in series. Each six-pulse bridge (rectifier or inverter) is connected to an AC system through a three-phase transformer. The transformers are connected in star/star and star/delta arrangement to provide phase displacement by 30 degrees. The characteristic of the harmonics generated by the six-pulse bridge in the case of normal operation are odd harmonics (5th, 7th, 11th, 13th, 17th, 19th, 23th, 25th, etc.). Therefore, the advantages of the 12-pulse HVDC converter unit are: increasing the DC output voltage to twice and eliminating the six-pulse DC voltage harmonic and odd harmonics (5th, 7th, 17th, 19th, etc.) of the AC currents on the DC and AC sides of the 12-pulse HVDC converter unit.

The 12-pulse HVDC converter unit has harmonic orders of (11th, 13th, 23th, 25th, etc.) on the AC side, and (12th) on the DC side (Kim *et al.*, 2009). These harmonics caused serious problems in the HVDC system, such as the Total Harmonic Distortion (THD) factor of AC current of the 12-pulse HVDC converter unit is 8.8% of fundamental current (Shah, 2013). Therefore, the 12-pulse HVDC converter unit does not meet power quality standard requirement determined by IEEE Standard (IEEE Std 519, 2014). For eliminating these harmonics, the HVDC system needs to provide additional filters at AC-side and DC-side of each 12-pulse HVDC converter unit. These filters are bulky in size and add approximately 10% of the cost of the HVDC system (Rudervall *et al.*, 2000; Kim *et al.*, 2009; Wang and Redfern, 2010).

According to the IEEE standard (IEEE Std 1030, 1987) and IEC standard (Zehong, 2011), HVDC systems can be classified into Mono-pole System (1PS), Bi-pole System (2PS), and Back-to-Back System (BTBS) topologies. The basic HVDC transmission is 1PS topology, which involves one or more 12-pulse HVDC converter

units in series or parallel on each side of the HVDC transmission line. Both converter (rectifier and inverter) neutrals are connected through a conductive medium, such as ground/sea HVDC electrode or metallic return for its current return path. According to the IEC standard (IEC 60050-195: 1998, 195-02-01), the definition of the HVDC electrode is a structure with a conductor or a group of conductors embedded in the soil or immersed in seawater, directly or surrounded with a specific conductive medium, providing an electric connection to the earth at rectifier side and inverter side.

The 2PS topology involves two parallel 1PS, one positive and one negative, with common HVDC ground/sea electrode or metallic return. The advantage of 2PS is the two 1PSs can be operated independently if one 1PS is on the outage, then the other 1PS can operate with 50% of its original system power capacity. According to IEEE Standard (IEEE Std 1030, 1987), for the reliability of power transmission the 2PS with ground/sea electrode or metallic return topology provides an effect equivalent to a two circuits HVAC transmission. Therefore, the major applications of 2PS topology is transmitting large electric power over long distance, for example, China has Yunnan-Guangdong 2PS LCC-HVDC link with 1438 *km* overhead lines and power rating of 5000 *MW*, ± 800 *kV* DC (Siemens, 2012; Huang *et al.*, 2009). The 2PS topology is also applied for long submarine transmission cables, such as Spain-Mallorca island LCC-HVDC link with 250 *km* lengths of cable and power rating of 400 *MW*, ± 250 *kV* DC (Siemens, 2012). As well as the 2PS topology is used for an exchange of power between two asynchronous AC systems, for example, the UK-France cross-channel LCC-HVDC link with 45 *km* lengths of cable and power rating of 2000 *MW*, ± 270 *kV* DC (Yates, 1982).

In BTBS, the DC side of the both rectifier and inverter are interconnecting directly without HVDC transmission lines and the whole BTBS is located in the same location (Kim *et al.*, 2009; Siemens, 2011; Benasla *et al.*, 2018). The BTBSs are used to interconnect two asynchronous AC systems, for example, Canada-USA BTB HVDC link with a power exchanging about 1000 MW, 145kV (Siemens, 2012).

The ground/sea HVDC electrode or metallic return is an essential part of the existing HVDC topologies for its current return path. This results in an additional cost to the HVDC transmission. Besides the costly presence of the HVDC electrode or metallic return in the existing HVDC power systems, the HVDC electrode producing severe adverse effects on the environment and the AC power systems nearby (Hu *et al.*, 2014; Kim *et al.*, 2009). To avoid this disadvantages of the existing HVDC topologies, in this study, a new four-pole HVDC transmission topology based on an LCC technology is proposed. The proposed topology consists of four HVDC transmission conductors without using HVDC electrode or metallic return. Such a system topology is called a Four-Pole System (4PS). Besides the absence of the HVDC electrode or metallic return in the proposed 4PS, the electrical power can be transferred through four effective parallel 12-pulse HVDC circuits instead of only two 12-pulse HVDC circuits with a common electrode or metallic return as in the existing 2PS topology. In this study, the operational concepts of the proposed system are illustrated, and the differences between the proposed 4PS and the conventional 2PS are analysed. Upgrading of the existing HVDC transmission system with 2PS topology to the 4PS topology. The proposed 4PS concepts have been verified by simulation with a full-scale model using MATLAB/Simulink software, as well as by experimental with a downscaled setup using a laboratory prototype. The conventional 2PS is used in this study as the standard reference for the comparison.

1.2 Problem Statement

According to the IEEE standard (IEEE Std 1378-1997), HVDC systems have been developed to transfer the electrical energy where HVAC transmission may not be the preferred choice or the most economical solution. According to IEEE Standard (IEEE Std 1030, 1987), for the reliability of power transmission, the 2PS with ground/sea electrode or metallic return topology provides an effect equivalent to two circuits of the HVAC transmission. Furthermore, according to the International Council on Large Electric Systems (CIGRE) guidelines for HVDC electrode design (675-2017) (Hu *et al.*, 2014), HVDC electrodes have been installed on HVDC transmission systems to provide a low resistance current return path during normal or outage mode operation, using the ground and/or sea as the conductive medium instead of the metallic return. This results indicate less cost and lower power losses than dedicated metallic return conductor. In addition, according to the International Electrotechnical Commission (IEC) standard (IEC/PAS 62344:2007) (Zehong, 2011), the HVDC electrode or metallic return of the HVDC transmission topologies must be able to carry the rated system current continuously. Moreover, with increasing the construction of HVDC transmission schemes in the world using the ground/sea as the conductive medium for its current return path result in more and more DC currents flowing in the earth (Rudervall *et al.*, 2000; Pierri *et al.*, 2017; Siemens, 2012). The DC current flows into the ground or sea can introduce severe adverse effects in an area extending to a radius of 10-60 of kilometers around each HVDC electrode (Siemens, 2011; Hu *et al.*, 2014). These adverse effects include electric and magnetic fields producing around the HVDC electrode when large DC current flow through earth or sea. According to (Kim *et al.*, 2009), to prevent electric shock hazards to animals and human beings, electric field strength, which occurs on the surface should not exceed

20 V/m for ground electrodes and 3 V/m for sea electrodes. Also, the magnetic field produced by electrode can cause a deviation from the earth magnetic field and causes an error in the compass of the ships nearby (Hu *et al.*, 2014). The effect of corrosion on the buried metallic structures is another adverse effect. According to (Hu *et al.*, 2014), the 0.01 A/m^2 of current density flow in the ground can cause electrolytic on buried metals embedded in the earth (i.e., cable sheaths and pipelines, among others). For example, the corrosion loss in the iron is 0.01162 mm per year. The DC bias of the AC power transformers is another adverse effect caused by the HVDC electrode. The DC current flowing through AC power transformers if their neutral points are grounded, which can cause the asymmetric magnetic core saturation during a sinusoidal half-period (Biro *et al.*, 2014; Pan *et al.*, 2016a). When operating in the half-cycle saturation condition, a transformer presents an increased the harmonic (Kefalas and Kladas, 2010; Hasegawa *et al.*, 2000), audible noise (He *et al.*, 2012), acute vibration of the transformer (He *et al.*, 2012; Ding *et al.*, 2016), and reactive power absorption (Kefalas and Klados, 2010; Kefalas and Kladas, 2012), which results in increased power losses, and consequently, overheating (Picher *et al.*, 1997).

Therefore in this study, to avoid the above disadvantages of the existing LCC-HVDC transmission topologies, a new 4PS HVDC transmission topology based on an LCC technology is proposed. The proposed topology consists of four effective parallel poles without using HVDC ground electrode or metallic return. Therefore, in the proposed 4PS the electrical power can be transferred through four effective 12-pulse HVDC circuits instead of only two 12-pulse HVDC circuits as in the existing 2PS topology. This upgrade results in eliminating HVDC ground electrode or metallic return and its disadvantages, on the one hand, and increasing the power density and system reliability, on the other.

1.3 Objectives

Objectives of this thesis are:

- i) To propose an improved LCC HVDC transmission system based on 4PS topology.
- ii) To investigate the reliability and power density of the proposed 4PS topology.
- iii) To compare and evaluate the performance of the proposed 4PS topology with the conventional 2PS topology.

1.4 Scope of the Thesis

The scope of this thesis is to introduce a new concept in the HVDC transmission by proposing a new 4PS topology without the required HVDC ground electrode or metallic return. This improvement of the HVDC transmission topology based on LCC technology that employing thyristor valves, emphasizing LCC-HVDC system applications for managing electrical power transfer between two AC power systems with different frequencies. The thesis is limited to study the operating principles and mathematical analysis of the proposed 4PS topology. The performance of existing AC and DC systems is compared. The overall system cost is not considering directly but has been focused on determine overall cumulative size of conductors of the 4PS over the 2PS under the same power transmitting and line losses. Verify the 4PS concepts by full-scale simulation model result and experiments on a downscaled setup result. A MATLAB/Simulink software and laboratory prototype are used for this purpose. The mathematical analysis, simulation model, and laboratory prototype of the conventional 2PS LCC-HVDC system are used in this study as the standard reference for the comparison with the proposed system.

1.5 Thesis structure

This thesis consists of five chapters, this chapter starts with describes the history of development the HVDC transmission and basic types and topologies of the HVDC system. also, describes clearly the objectives and scope of the research.

In Chapter 2, the performance of existing HVAC and HVDC electric power systems are compared via a literature review. This chapter also illustrates the topologies and its operation modes of existing LCC-HVDC systems as well as, types of electrodes used in existing HVDC topologies and its impacts on the environment, such as corrosion, soil overheating, and groundwater heating and impacts on the AC power systems nearby are described and presented.

Chapter 3 covers the methodology for the design aspects of the proposed system done in this research. System design includes the following aspects which are described in the body of the chapter: design criteria, operating concepts, mathematical model, simulation, and experimental work.

Chapter 4 presents all the obtained results which include: (i) mathematical and analytical results which are the contributions of the proposed 4PS and comparison of these results with the conventional 2PS. (ii) Simulation results which are in normal mode operation, mono-pole (in the 2PS) and bi-pole (in the 4PS) failure modes operations, and AC line-to-ground fault at the inverter side in both 2PS and 4PS. (iii) The THD results of the AC line current on the AC sides of the 12-pulse HVDC converters (rectifier and inverter). (iv) Experimental results of the conventional 2PS, the proposed 4PS, and the comparison of these two results. The last Chapter gives conclusion and suggestion of future works.

CHAPTER 2

LITERATURE REVIEW

2.1 Overview

In this Chapter, the performance of existing HVAC and HVDC electric power systems are presented in detail via a literature review. This chapter also illustrates the main components of an HVDC power system which are 12-pulse HVDC converter unit, HVDC transmission medium, and HVDC electrode. Furthermore, the types of HVDC electrodes used in the existing HVDC transmission systems are presented. Highlighting the impacts of the HVDC ground/sea electrode on the environment and the AC power systems nearby. Finally, the topologies and their operating modes of existing LCC-HVDC systems are described and presented.

2.2 The performance comparison of existing AC and DC systems

The voltage level in the DC system can be designed equivalent to the peak value of the voltage level in the AC system (Lucas, 2001). Thus, for the same amount of insulation between line voltage and ground, the ratio of DC voltage to the RMS value of the AC voltage is $\sqrt{2}$ (Weedy *et al.*, 2012).

$$V_d = V_p = \sqrt{2} V_{rms} \quad (2.1)$$

Where, V_p , V_{rms} and V_d are peak value and RMS value of the AC voltages, and DC voltage, respectively.

For the same resistivity of conductor material and the same conductor size, the same current can carrying with both DC and AC, if skin effect is not considered (Lucas, 2001). Thus, the following equations are addressed:

$$i_d = i_p = \sqrt{2} i_{rms} \quad (2.2)$$

$$R_{dc} = R_{ac} \quad (2.3)$$

Where, i_d, i_p, i_{rms} are DC line current, peak and RMS values of the AC line current, respectively, R_{dc}, R_{ac} are resistance of the DC and AC conductors, respectively.

In practice, the AC power system is carried out using the three-phase system with three conductors and DC power system using 2PS with two conductors. Thus, the ratio of DC power P_{dc} over AC power P_{ac} can be calculated as Equation (2.4)

$$\frac{P_{dc}}{P_{ac}} = \frac{2 V_d i_d}{\sqrt{3} V_{rms} i_{rms} \cos \phi} = \frac{2(\sqrt{2} V_{rms} \sqrt{2} i_{rms})}{\sqrt{3} V_{rms} i_{rms} \cos \phi} = \frac{4}{\sqrt{3} \cos \phi} \quad (2.4)$$

It means that the capabilities of power transmission of a DC system with two conductors and an AC system with three conductors are 2.44 times if $\cos \phi = 0.945$ (Lucas, 2001). Therefore, the ohmic losses can be compared in both AC and DC systems as Equation (2.5) (Kamakshaiah and Kamaraju, 2011):

$$\frac{W_{dc}}{W_{ac}} = \frac{2 i_d^2 R_{dc}}{3 i_{rms}^2 R_{ac}} = \frac{2\sqrt{2} i_{rms}^2 R_{ac}}{3 i_{rms}^2 R_{ac}} = 0.9428 \quad (2.5)$$

Where, W_{dc}, W_{ac} are DC and AC power losses. From Equation (2.5), for same power transmitting, the percentage line losses by DC system (2PS) is reduced to 94.28 % in comparison with the three-phase AC system.

The power transfer mechanism of the conventional AC power system is predominantly inductive and has traditionally been grouped into three separate parts, which are a generation, transmission, and distribution, all of them inflexibly tied by the synchronous constraints. The presence of inductance in the AC circuit results in phase shifts between the voltage and current waveforms which affect the power transfer

efficiency (Arrilaga *et al.*, 2007). By contrast, in the DC systems, the frequency is zero, hence the inductance and capacitance parameters do not have an effect on the power transfer efficiency (Siemens, 2011). Thus, the impedance Z of the HVAC transmission line is $Z = R_{ac} + jx$, where x is reactance, and this impedance is reduced down to only R_{dc} in the case of HVDC line (Kalair *et al.*, 2016). Figure 2.1 (a) and (b) shows the AC and DC transmission lines, respectively, interconnecting two ideal AC voltage sources V_{p1} and V_{p2} . The AC line with a pure inductance X_L and DC line with a pure resistance. Thus, the maximum power flow in the HVAC and HVDC lines is limited by Equations (2.6) and (2.8), respectively.

$$P_{ac} = \frac{V_{p1} V_{p2} \sin \delta}{X_L} \quad (2.6)$$

$$Q_{ac} = \frac{V_{p2}(V_{p1} \sin \delta - V_{p2})}{X_L} \quad (2.7)$$

$$P_{dc} = \frac{V_{d1}(V_{d1} - V_{d2})}{R_{dc}} \quad (2.8)$$

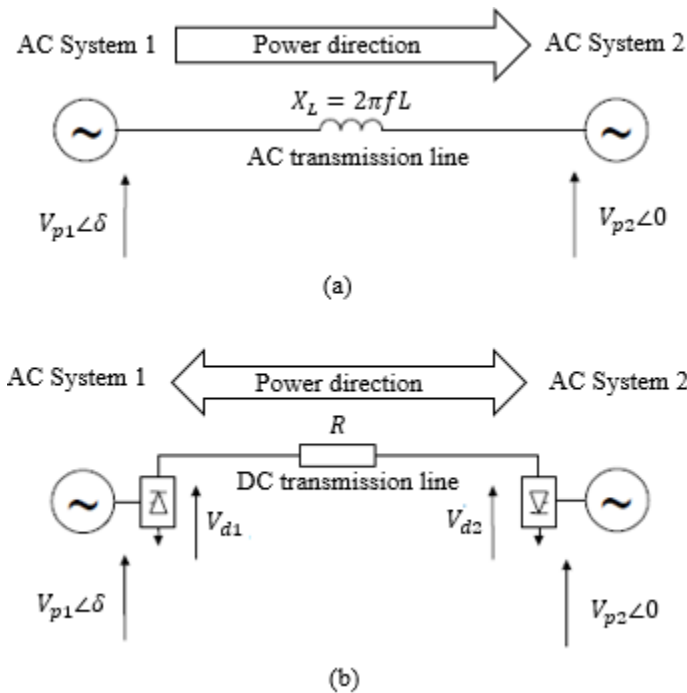


Figure 2.1 The power transfer mechanism of (a) the AC line and (b) DC line

Where, $\sin \delta$ is the voltage phase angle between sending end and receiving end of the HVAC transmission line. Usually, the HVAC systems are operated below $\delta = 30^\circ$ due to stability issue (Kalair *et al.*, 2016). Whereas, the loss of power in the DC line is an ohmic loss only. A recent study (Pickard, 2013) found that the maximum distance of the HVDC systems for transmitting electrical power with a 2% loss of its capacity is limited by line length of less than 10000 *km*.

According to ABB review in (Claes *et al.*, 2014), the AC cables have large capacitive characteristics (see Figure 2.2 (a)), whereas AC overhead lines have large inductive characteristics (see Figure 2.2 (b)). The presence of capacitive in the AC circuit results in a continuous loss because of charging current even though the load is open. The DC circuit, as opposed to AC, do not generate reactive power. Thus, the power transmission capacity by cables (Figure 2.2 (c)) or overhead lines (Figure 2.2 (d)) in a DC system is constant with distance. By contrast, in AC system the power transmission capacity is reduced with increasing line length as shown in Figure 2.2 (c) and (d).

Another technical comparison result between three-phase double-circuit 400 *kV* AC system and 500 *kV* HVDC 2PS system based on the loadability characteristics at the thermal limit of the transmission lines is presented in (Lauria *et al.*, 2014a; Lauria *et al.*, 2014b), where this result is reported in Figure 2.3. The Figure shows that the conventional 2PS with two conductors overhead lines allows the largest capacity of power transmission for line lengths of more than 500 *km*. Whereas, double-circuit AC with six conductors overhead lines allows the largest capacity of power transmission for a line length of less than 140 *km*. Therefore, the best loadability performances are obtained through a DC power to AC power ratio.

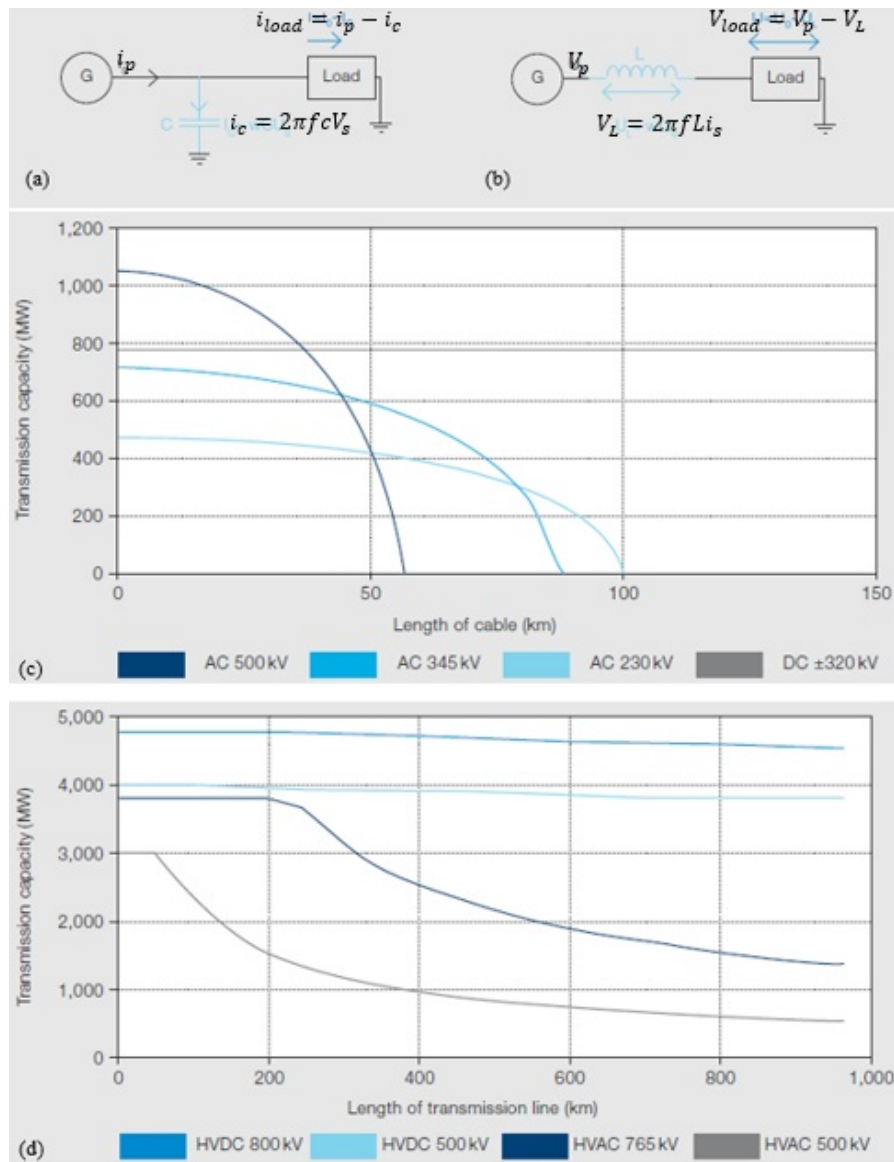


Figure 2.2 (a) capacitive characteristics of AC cable, (b) inductive characteristics of AC overhead line, (c) transmission capacity of AC and DC systems with underground cables, and (d) with overhead lines (Claes *et al.*, 2014).

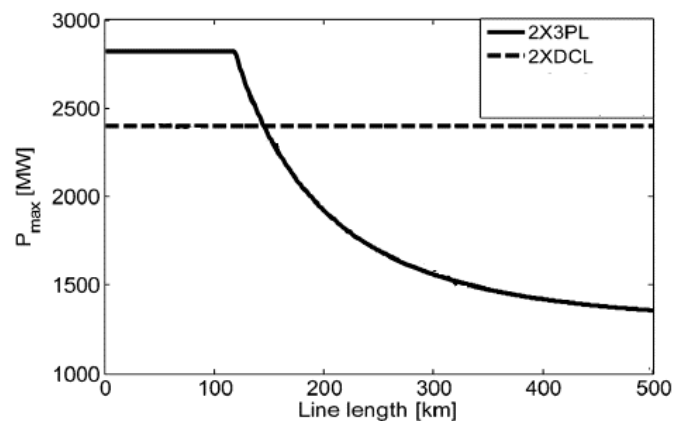


Figure 2.3 The loadability characteristics of the three-phase double-circuit AC system ($2 \times 3PL$) versus 2PS HVDC system ($2 \times DCL$) (Lauria *et al.*, 2014b).

2.3 Main Components of an HVDC Power System

HVDC power system refers to that the AC power at the transmitting side is converted into DC power before its transmission. At the receiving side, it is then converted back into its original AC power and then supplied to users (Andersen, 2006; Kim *et al.*, 2009). The HVDC systems are used to transmit bulk power over long distance by cables and/or overhead lines and for interconnecting asynchronous AC systems having the same or different frequency (Pierri *et al.*, 2017; Benasla *et al.*, 2018; Sun *et al.*, 2017). Figure 2.4 (a) shows an LCC HVDC transmission system with the basic principle of transferring electric power from AC system 1 to AC system 2 or vice versa (Setreus and Bertling, 2008; Pierri *et al.*, 2017; Benasla *et al.*, 2018). The following three main components are necessary to define an LCC HVDC system.

2.3.1 12-Pulse HVDC Converter Unit

According to the IEEE Standards (IEEE Std 1378, 1997; IEEE Std 1030, 1987), the 12-pulse HVDC converter unit with three quadruple thyristor valves is used in LCC HVDC converter units as shown in Figure 2.4 (b). Each thyristor valve is a series connection of a certain number of thyristors as shown in Figure 2.4 (c). Therefore, each converter station at ends of the HVDC transmission system is built as one or more 12-pulse HVDC converter unit (Siemens, 2011). The converter stations at each end of an HVDC link are replicas of each other and operates as a rectifier which converts AC power to DC or an inverter which converts the DC power to AC. The rectifier and inverter converter stations are interconnected through HVDC conductive medium (e.g. overhead lines, underground cable, submarine cable, short busbar link) (Pierri *et al.*, 2017). The 12-pulse HVDC converter unit can be operated either as a rectifier station or an inverter station. The change from the rectifier to inverter action and vice versa is

smoothly obtained by control of firing angle α (Weedy *et al.*, 2012). In the LCC systems, the current can flow in one direction only, therefore, the power reversal is achieved by a converter polarity reversal (Andersson *et al.*, 2015). As a result, the direction of power flow in the LCC system can be bi-directionality depending on the application and location of the HVDC systems (Rudervall *et al.*, 2000). For example, the rectifier and inverter converter stations exchange roles if a reversal of power flow is required. Figure 2.4 (b) shows a typical 12-pulse HVDC converter unit consists of two six-pulse bridges connected in series on the DC side. Each six-pulse bridge is supplied by secondary windings of three-phase AC transformers. Whereas, the primary windings of the transformers are connected in parallel and supplied by the AC system (Arrilaga *et al.*, 2007; Kim *et al.*, 2009). Converter transformers can be arranged in the following configurations as shown in Figure 2.4 (d), which are: (i) one (three-phase/three-winding) transformer; (ii) two (three-phase/two-winding) transformers; (iii) three (single-phase/three-winding) transformers; (iv) six (single-phase/two-winding) transformers. This arrangement of 12-pulse HVDC converter unit (as in Figure 2.4 (b)) is necessary for eliminating current harmonics on the AC side and cancel out six-pulse voltage harmonics on the DC side (Siemens, 2011).

According to (Weedy *et al.*, 2012; Lucas, 2001) agree that the mean DC voltage with polarity output of the six-pulse rectifier bridge V_{d_R} and inverter bridge V_{d_I} are given by Equations (2.9) and (2.10), respectively:

$$V_{d_R} = (3\sqrt{2}/\pi) V_{LL} \cos(\alpha_R) - R_{C_R} i_d \quad (2.9)$$

$$V_{d_I} = (3\sqrt{2}/\pi) V_{LL} \cos(180^\circ - \alpha_I) + R_{C_I} i_d \quad (2.10)$$

Where, V_{LL} is line-to-line AC voltage, $R_{C_R} i_d$ and $R_{C_I} i_d$ are voltage drop in the transformer leakage inductance of rectifier side L_R and inverter side L_I , respectively.

$$R_{C,R} i_d = \frac{3 \omega L_R}{\pi} i_d \quad (2.11)$$

$$R_{C,I} i_d = \frac{3 \omega L_I}{\pi} i_d \quad (2.12)$$

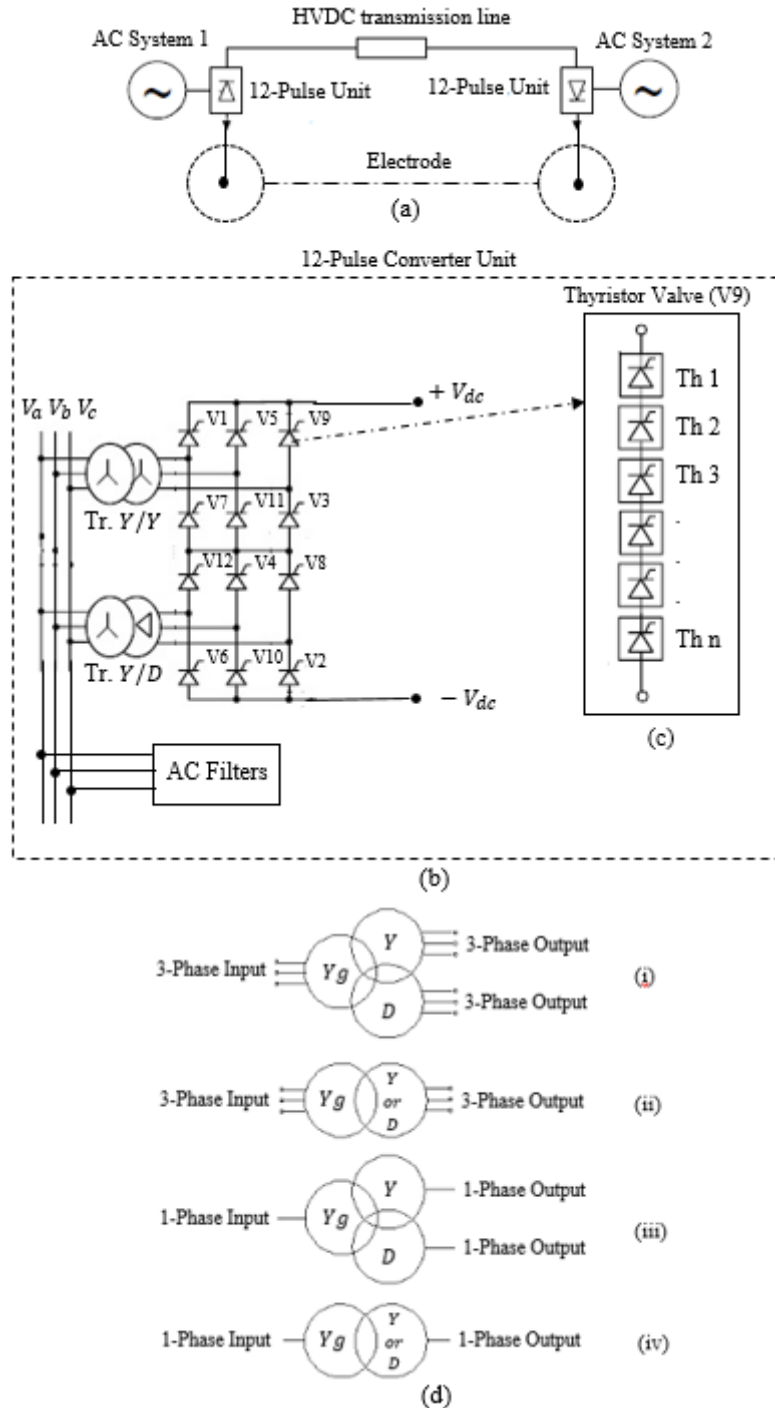


Figure 2.4 LCC HVDC system (a) Main Components, (b) 12-pulse HVDC converter unit, (c) Thyristor valve, and (d) arrangements of the transformer (Kim *et al.*, 2009; Siemens, 2011)

In the conversion process, the converter (rectifier and inverter) producing AC and DC harmonics. Figure 2.5 shows typical DC voltage and AC current waveforms with harmonics for a 12-pulse HVDC converter unit. From Figure 2.5 (a), the DC voltage of each six-pulse bridge has a ripple component at six times the fundamental frequency. The summation of the two six-pulse DC voltages results in cancel six-pulse voltage ripple, leaving a component that repeats at 12 times per cycle. Figure 2.5 (b) illustrates the AC currents on the AC-side of the 12-pulse HVDC converter unit. Each six-pulse current (non-sinusoidal) flowing in the primary-winding of the transformer has a rectangular waveform. The summation of these two six-pulse currents results in the acceptable sinusoidal waveform as the fundamental components (Kim *et al.*, 2009).

The harmonic order h on the AC side of the converter is $h = Kp \pm 1$, whereas, on the DC side is $h = Kp$. Where, p is the converter pulse number and k is positive integer. The non-sinusoidal waveforms of the six-pulse converter line current may be expressed as a Fourier Series (Weedy *et al.*, 2012; Kim *et al.*, 2009). Thus, the six-pulse bridge line current $i_{p(Y/Y)}$ for wye/wye transformer connection is:

$$i_{p(Y/Y)} = \frac{2\sqrt{3}}{\pi} i_d \left[\sin \omega t + \frac{1}{5} \sin 5\omega t + \frac{1}{7} \sin 7\omega t + \frac{1}{11} \sin 11\omega t + \frac{1}{13} \sin 13\omega t + \dots \right] \quad (2.13)$$

The six-pulse bridge line current $i_{p(Y/D)}$ for wye/delta transformer connection is:

$$i_{p(Y/D)} = \frac{2\sqrt{3}}{\pi} i_d \left[\sin \omega t - \frac{1}{5} \sin 5\omega t - \frac{1}{7} \sin 7\omega t + \frac{1}{11} \sin 11\omega t + \frac{1}{13} \sin 13\omega t + \dots \right] \quad (2.14)$$

In the 12-pulse HVDC converter unit, the AC current is the sum of the currents $i_{p(Y/Y)}$ and $i_{p(Y/D)}$. Thus, the following equation can be written (Kim *et al.*, 2009):

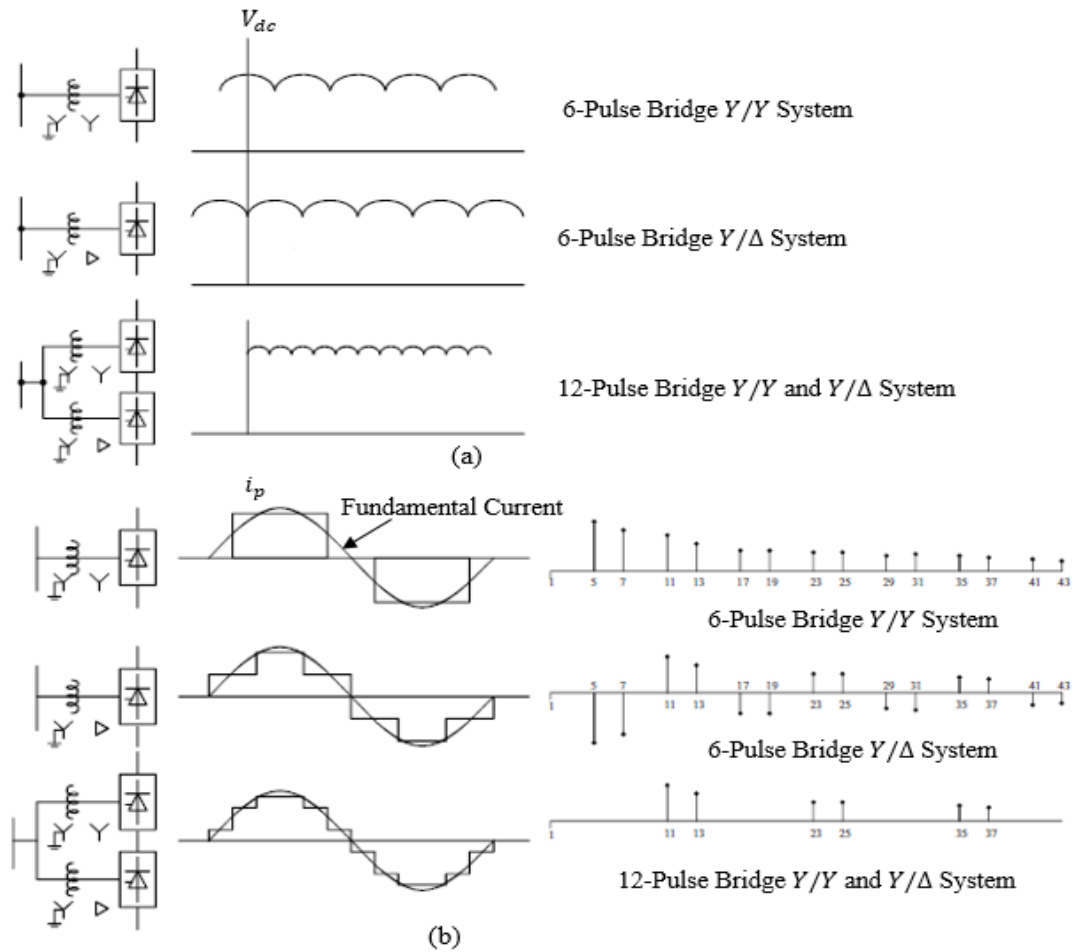


Figure 2.5 Voltage and current waveforms of a 12-pulse HVDC converter unit: (a) DC voltage waveform, (b) AC current waveform with harmonics (Kim *et al.*, 2009).

$$\begin{aligned}
 & i_p(Y/Y) + i_p(Y/D) \\
 &= \frac{4\sqrt{3}}{\pi} i_d \left[\sin \omega t + \frac{1}{11} \sin 11\omega t + \frac{1}{13} \sin 13\omega t \right. \\
 & \quad \left. + \frac{1}{23} \sin 23\omega t + \frac{1}{25} \sin 25\omega t + \dots \right] \tag{2.15}
 \end{aligned}$$

In the Equation (2.15), the harmonics of opposite polarity per cycle is canceled out. Therefore, in a typical 12-pulse HVDC converter unit the AC current harmonics have orders of (11th, 13th, 23th, 25th, etc.) on the AC side, whereas, on the DC side the DC voltage harmonic have an order of (12th). To improve the power quality and meet the IEEE Standard (IEEE Std 519-2014) requirements, filters at AC harmonics 11th, 13th,

23rd, and 25th are required on the AC side of a 12-pulse HVDC converter unit (Shah, 2013; IEEE Std 519, 2014). Whereas, a large inductor (smoothing reactor) is connected between the converter unit and each DC line to smooth the DC current and for the converter protection from DC line faults (Siemens, 2011; Rashid, 2017).

Fig. 2.6 shows a typical variation of the reactive power Q demand versus active power P of an LCC HVDC converter; the reactive power demand is shown to be approximately 50 % of the power transmitted at full load (Arrilaga *et al.*, 2007). Therefore, for providing this reactive power the capacitor banks are used at the AC side of each converter. The shunt capacitor banks and AC filters occupy a large area of the converter station and add approximately 10% of the cost of the HVDC system (Rudervall *et al.*, 2000; Wang and Redfern, 2010). The large capacitance of shunt capacitor banks and AC filters can result in large AC over-voltages in weak AC grids during fault recovery (Adam and Williams, 2016). For this reason, an LCC HVDC scheme needs to be connected to a strong AC system with the Short Circuit Ratio (SCR) of at least 2.5 (Andersen, 2006).

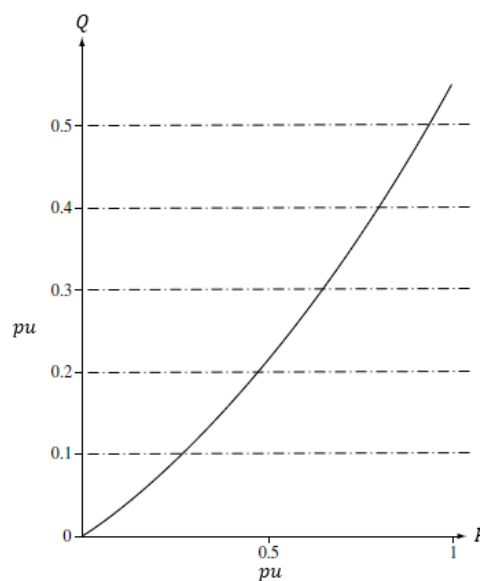


Figure 2.6 Variation of reactive power with active power (Arrilaga *et al.*, 2007)